Airway injury induces alveolar epithelial and mesenchymal responses mediated by macrophages

Irene G. Wong[1,2], Jillian Stark[2,3,*], VanNashlee Ya[2,*], Aaron L. Moye[2], Alan Baez Vazquez[1,4,5], Susanna M. Dang[1,2], Andrea Shehaj[2], Maral J. Rouhani[6], Roderick Bronson[7], Sam M. Janes[6], Samuel P. Rowbotham[2,8], Margherita Paschini[2], Ruth A. Franklin[5,9], Carla F. Kim[2,9,10]

Affiliations:
[1]Harvard University, Cambridge, MA 02138, USA
[2]Stem Cell Program, Division of Hematology/Oncology and Pulmonary & Respiratory Diseases, Children's Hospital Boston, Boston, MA 02115, USA; Department of Genetics, Harvard Medical School, Boston, MA 02115, USA
[3]Harvard College, Cambridge, MA 02138, USA
[4]Department of Molecular and Cellular Biology, Harvard University, Cambridge, MA 02138, USA
[5]Department of Stem Cell and Regenerative Biology, Harvard University, Cambridge, MA 02138, USA; Department of Immunology, Harvard Medical School, Boston, MA 02115, USA
[6]UCL Respiratory, Division of Medicine, University College London, London, UK
[7]Rodent Histopathology Core, Harvard Medical School, Boston, MA 02115, USA
[8]Pediatric Surgical Research Laboratories, Mass. General Hospital, Boston MA 02114 USA. Department of Surgery, Harvard Medical School, Boston MA 02115
[9]Harvard Stem Cell Institute, Cambridge, MA 02138, USA
[10]Corresponding author: carla.kim@childrens.harvard.edu
*Authors contributed equally

Highlights

- Airway epithelial cell injury causes proliferation of AT2 cells, the alveolar epithelial progenitor cells

- Alveolar macrophages promote AT2 cell proliferation after airway injury via upregulation of *Spp1*
- Alveolar macrophages have a pro-fibrotic effect on lung mesenchyme after airway injury
- Damage to one epithelial compartment can elicit altered epithelial- immune-mesenchymal cell crosstalk in another compartment of the same tissue

Summary

Acute injury in the airways or the lung activates local progenitors and stimulates changes in cell-cell interactions to restore homeostasis, but it is not appreciated how more distant niches are impacted. We utilized mouse models of airway-specific epithelial injury to examine secondary tissue-wide alveolar, immune, and mesenchymal responses. Single-cell transcriptomics and *in vivo* validation revealed transient, tissue-wide proliferation of alveolar type 2 (AT2) progenitor cells after club cell-specific ablation. The AT2 cell proliferative response was reliant on alveolar macrophages (AMs) via upregulation of *Spp1* which encodes the secreted factor Osteopontin. A previously uncharacterized mesenchymal population we termed Mesenchymal Airway/Adventitial Niche Cell 2 (MANC2) also exhibited dynamic changes in abundance and a pro-fibrotic transcriptional signature after club cell ablation in an AM-dependent manner. Overall, these results demonstrate that acute airway damage can trigger distal lung responses including altered cell-cell interactions that may contribute to potential vulnerabilities for further dysregulation and disease.

Introduction

Across diverse tissues, injury and disease states can promote a cellular response that occurs locally to repair damaged tissue or which may be a general systemic response from distant sites. Pneumonectomy, or removal of a lung lobe, results in tissue-wide compensatory growth in the remaining lobes in mammals[1,2]. Regenerative responses in uninjured, distant niches have been observed in other organs and organisms[3]. For example, muscle injury to one leg of a mouse can stimulate an activated cell cycle state in the uninjured contralateral limb[4], and limb amputation or limb crush in axolotls could

similarly induce proliferation throughout the uninjured contralateral limb[5]. The lungs are composed of different epithelial cell types that have been described to act as stem/progenitor cells in their local niche, at the location of injury. The lungs initiate regenerative responses to homeostatic disruptions, but it is not known if or how local epithelial injuries can affect changes in more distant epithelia throughout the organ. This may be particularly relevant for complex lung injuries, infections and diseases like environmental exposures, chronic obstructive pulmonary disease, COVID-19, and lung cancer which exhibit dysfunction across different niches of the lungs, from the upper airways, small airways, to alveoli[6].

The distal adult lung is composed of airways and alveoli that facilitate gas exchange, and injuries or diseases that perturb these regions can disrupt normal lung function and stimulate the activity of facultative progenitor cells. In human and mouse lungs, club cells are epithelial stem cells that help maintain the airway barrier and self-renew and differentiate in the event of airway injury[7]. Mouse models demonstrated that club cells can differentiate into ciliated cells[8,9], and in certain severe injury contexts using bleomycin or influenza, club cells can differentiate into alveolar type 2 (AT2) cells[10]. Studies utilizing murine models of airway injury and repair are focused primarily on local responses around the airways[11], and thorough characterization of responses in the alveolar region is absent. The alveolar region contains AT2 epithelial cells that can self-renew and differentiate into alveolar type 1 (AT1) cells[7]. Whether and how AT2 cells are affected by airway injuries in the proximal or distal lung is unknown.

Club cells and AT2 cells have been described to be regulated within their bronchiolar and alveolar niches, respectively, by diverse cell types and factors, such as immune and mesenchymal cells. CCR2+ monocytes are required for AT2 cell proliferation after pneumonectomy and tracheal epithelial repair after polidocanol injury[12,13]. After club cell specific naphthalene airway injury, F4/80+ macrophage/monocytes increase in the lungs[14,15] and depletion of alveolar macrophages (AMs) during the regenerative phase impaired airway repair[14]. Among the lung mesenchyme, fibroblast populations expressing Pdgfrα support the culture and differentiation of AT2 cells in alveolosphere

assays and are composed of subpopulations that can be distinguished based on their additional expression of Wnt2 or Axin2[7,16,17]. Pdgfrα+/Axin2+ mesenchymal cells, termed mesenchymal alveolar niche cells (MANCs), secrete factors such as Fgf7 and Il6 to maintain the alveolar niche[17]. Additionally, severe club cell airway injury from repeated weekly naphthalene injury or repeated genetic depletion of club cells results in peribronchiolar fibrosis[18,19]. The effects of airway injury on alveolar-supportive mesenchyme, or how immune cells stimulated by airway epithelial defects may impair the alveolar space however, are unknown.

Here, we sought to identify tissue-wide changes to airway injury and characterize the cell-cell interactions that mediate these responses. We performed single-cell RNA sequencing (scRNA-seq) to interrogate *in vivo* alveolar responses to naphthalene-mediated club cell injury and discovered a proliferative AT2 cell response that was also conserved in a genetic club cell injury model. We then identified alveolar macrophages as regulators of this proliferation response, characterized by upregulation of *Spp1*, the gene that encodes for Osteopontin. *Spp1*+ macrophages, previously associated with fibrosis of lung, heart, liver and other organs[20], were found to modulate a population of Sca1-/CD34+ fibroblasts we termed Mesenchymal Airway/Adventitial Niche Cell 2 (MANC2) cells due to their transcriptional similarities yet also distinctions from the previously described MANCs. In the absence of alveolar macrophages, the AT2 cell proliferation and MANC2 responses were attenuated. Overall, our work reveals alveolar macrophages as drivers of previously underappreciated tissue-wide responses to acute airway injury, underscoring the potential for further dysregulation upon additional, more complex lung injuries.

Results

Transient proliferation of AT2 cells after naphthalene airway injury

In order to study tissue-wide effects of airway injury, we performed single cell RNA-seq on mouse lung epithelium from the naphthalene club cell injury model. We treated adult mice with corn oil control or 200 mg/kg naphthalene. As expected, mice exhibited the highest loss of club cells at 2 days post-naphthalene, detected by the absence of

CCSP+ club cells in airways and flattening of ciliated cell projections, and club cells regenerated over a period of up to 21 days (Figure 1A-B, data not shown). We then performed scRNA-seq of sorted alveolar-enriched Sca1- epithelium and airway-enriched Sca1+ epithelium during the peak (day 2) and regenerative phases (day 7) after airway injury (Figure 1A, S1A). After filtering and removal of a low quality/dying cluster of AT2 cells (Figure S1B, see methods), cell clusters were annotated according to known marker genes for distal lung epithelial cell types[21] (Figure S1C). We identified major cell types of the airway, such as club cells and ciliated cells, and cell types of the alveolar space, such as AT2 cells and AT1 cells (Figure 1C). We annotated an "AT2/AT1" cluster of alveolar cells based on a gradient of low AT2 cell marker expression to high AT1 cell marker expression, which was present in all samples and independent of injury (Figure 1D,G, Figure S1A).

We used differential gene expression and Gene Ontology (GO) analysis to characterize epithelial cell changes after naphthalene. In club cells at day 2, we identified the upregulation of genes like *Il33* and biological processes such as "positive regulation of programmed cell death," reflective of the injury to club cells[14] (Table S1-2). In ciliated cells, *Wnt7b* was among the upregulated genes at the peak of injury, in agreement with previous findings on the surviving ciliated cells of the airway[22] (Table S1). At 7 days post-naphthalene, GO analysis of differentially expressed genes (DEGs) highlighted biological processes like "developmental process" and "multicellular organism development" in club cells and "cilium organization" and "cell projection assembly" in ciliated cells, indicative of the regenerating airway epithelium (Table S3-4). Surprisingly, subclustering of the alveolar epithelium in the scRNA-seq data suggested a larger proportion of proliferative AT2 cells after airway injury (Figure 1D-G). Because naphthalene is only metabolized by club cells that express Cyp2f2 and converted into toxic reactive oxidative species[23,24], changes to AT2 cells were not expected after injury. As expected in control lungs, Cyp2f2 was detected only in CCSP+ club cells but not in AT2 cells, suggesting that AT2 cells do not metabolize naphthalene (Figure S1D).

Immunofluorescence (IF) confirmed observations from the scRNA-seq, showing that AT2 cell proliferation is increased *in vivo* after naphthalene-mediated club cell injury. IF for the proliferation marker Ki67[25] and the AT2 cell marker SPC was performed at various time points. There was a transient increase in the fraction of proliferative AT2 cells (Ki67+ SPC+ cells) near the airways at days 2 and 7 after club cell injury (Figure 1H-I). To determine whether this effect was spatially restricted to alveoli near the airways or widespread throughout the lung, we expanded our analysis to include distal regions of the alveolar space. Proliferative AT2 cells were also transiently increased in the distal alveolar region, at days 2, 7, and 10 after injury and subsided by day 14 (Figure 1H, J). With lineage tracing of club cells using CCSP-driven Cre recombinase prior to naphthalene injury[26], we did not observe YFP+ club cells in the alveolar space of the lungs at day 7 after injury (Figure S1E-G). Thus, we concluded that AT2 cell proliferation observed after naphthalene-mediated club cell injury occurs in native AT2 cells. Furthermore, there was no increased abundance of alveolar cells with Krt8 in the naphthalene-treated animals, suggesting that naphthalene does not drive AT2 cells towards a transitional cell state[27–29] (data not shown).

Transient proliferation of AT2 cells after genetic club cell ablation

To determine whether AT2 proliferation is a conserved, biologic response after club cell injury and not an artifact of naphthalene injury, we used a genetic model of club cell ablation and corroborated our findings in the chemical model. In CCSP-CreER+/-; Rosa26-LSL-YFP/iDTR mice[30,31], tamoxifen induced expression of the diphtheria toxin receptor (iDTR) and YFP label on CCSP-expressing club cells (Figure S1E). We administered PBS (control) or diphtheria toxin-A (DT) via intratracheal injection to acutely deplete club cells in the lungs of these mice (Figure 2A). We confirmed that lineage labeling, also a proxy for iDTR, was confined to club cells and did not label any SPC+ AT2 cells on the day of injury (Figure S2A). IF determined that CCSP+ club cell injury peaked at day 2 after DT administration, with no other obvious histological changes in the injured state compared to the control (Figure 2B-C, Figure S2B-C). AT2 cell proliferation near airways was significantly increased at day 7 after club cell ablation (Figure S2D) and occurred as early as day 4 after ablation in the alveolar region (Figure

2D-E). These increases in AT2 cell proliferation were also transient, as these effects disappeared over the time course that corresponded with club cell restoration. Despite the differences in the severity and mechanism of club cell death between the naphthalene and genetic ablation models, these results demonstrate a conserved AT2 proliferation response to club cell depletion.

We next sought to use an organoid system to determine the potential driver(s) of AT2 cell proliferation after club cell injury. To test whether AT2 cell proliferation was a cell-autonomous behavior, we isolated Sca1- alveolar-enriched epithelium from control or naphthalene-treated mice for organoid co-culture[32] (Figure 2F). Alveolar organoid forming efficiency (OFE) was unchanged whether the epithelial cells were derived from injured or uninjured animals, suggesting that there may be cellular cues from the *in vivo* injured environment that are required to promote increased AT2 cell proliferation (Figure 2G-H).

<u>Alveolar macrophages mediate AT2 cell proliferation after airway injury</u>

Because AT2 cell proliferation occurred near airways and also throughout the alveolar space after club cell depletion, we hypothesized that these changes were mediated by immune cells, which are capable of rapid movement throughout tissues. Previous works using multiple lung injury models has demonstrated the importance of myeloid cells in promoting lung epithelial cell proliferation[33]. We therefore sought to interrogate the potential contributions of lung macrophages, composed of alveolar macrophages (AMs) and interstitial macrophages (IMs)[33], towards increased AT2 cell proliferation after club cell injury. We performed flow cytometry analysis on CD45+ immune cells from control and naphthalene-injured animals at multiple timepoints after injury (Figure 3A). We observed a significant increase of SiglecF+/CD11b- AMs in naphthalene-injured lungs at day 2 after injury, which correlated with a timepoint at which AT2 cell proliferation was observed (Figure 3B). Although not significant, we observed an upward trend in total CD64+ lung macrophage abundance at days 2 and 7 after injury (Figure S3A).

We next performed AM depletion *in vivo* and observed a loss of the AT2 cell proliferation response after airway injury. We pre-treated mice with PBS control liposomes or clodronate liposomes to deplete AMs prior to naphthalene injury and test its effects on AT2 cell proliferation[14,34,35] (Figure 3C). Flow cytometric validation of clodronate liposome-treated animals without injury confirmed that the reduction in AMs could be sustained for at least 2 weeks and therefore, the duration of the AT2 cell proliferation response after naphthalene (Figure S3B-C, Figure 1I-J). After clodronate liposome pre-treatment with and without injury, flow cytometry indicated that macrophages did not increase in response to naphthalene injury after AM depletion (Figure 3D, Figure S3D). Hematoxylin and eosin (H&E) staining of the pre-treated and injured lungs did not highlight obvious differences in the general lung morphology and structure (data not shown), and IF of naphthalene-treated animals indicated an approximately equal amount of club cell loss between PBS or clodronate treatment at day 7 after injury (Figure S3E). Subsequently, we examined AT2 proliferation after liposome pre-treatment, with and without naphthalene injury (Figure 3E). AM depletion with clodronate liposomes attenuated AT2 proliferation responses to naphthalene at day 7 after injury (Figure 3F, Figure S3F). These results suggest that AMs are essential cellular mediators of the alveolar proliferation response to naphthalene airway injury.

Next, we determined that AMs are sufficient to increase AT2 cell proliferation, as we observed an increase in alveolar organoid formation when AT2 cells were co-cultured with airway injury-exposed AMs. AMs from control or naphthalene-treated animals were isolated by bronchoalveolar lavage (BAL) at day 7 after injury during the peak of AT2 proliferation (Figure 1I-J). AMs are the predominant immune cell population in BAL fluid[14,36]. AMs were then enriched by magnetic activated cell sorting (MACS), and used for co-culture with naïve DsRed+ alveolar organoids in a growth factor-defined media[37] (Figure 3G, Figure S3G-H). AMs derived from the naphthalene-injured environment supported a higher OFE as compared to AMs from an uninjured environment (Figure 3H-I). These results suggest that AMs produce factors that can directly impart pro-proliferative effects on AT2 cells after naphthalene injury.

Alveolar macrophages upregulate *Spp1* during airway repair

We performed scRNA-seq on immune cells and identified secreted factors upregulated by AMs after naphthalene airway injury. scRNA-seq was performed on a 1:1 mixture of cells from BAL fluid (composed predominantly of AMs) and FACS-enriched CD45+ immune cells at days 2 and 7 after naphthalene injury (Figure 4A, Figure S4A). We identified major immune cell types of the lung using the PanglaoDB and other published works[38–40] (Figure 4B-C, Figure S4B, Table S5) and performed differential gene expression analysis on AMs at day 7 after naphthalene injury (Figure 4D). A subset of the DEGs were categorized in PANTHER as intercellular signaling molecules or transmembrane signaling receptors[41] including the most differentially expressed gene, *Spp1*, and *Ccl6*, and *Gpnmb*. Other DEGs were associated with metabolic processes (Figure S4C).

We subsequently identified Osteopontin (OPN), the protein encoded by *Spp1,* as one of the AM-secreted factors that could promote AT2 proliferation (Figure 4E). We measured the concentration of OPN in media reserved from the AM and alveolar organoid co-culture experiments (Figure 3G-I). Media from organoids grown with injury-exposed AMs demonstrated a significant increase in OPN concentration (Figure 4F). We then isolated AMs from uninjured and naphthalene-injured *Spp1* knockout (-/-) mice[42] to determine whether there would be any differences in the AMs' ability to promote increased alveolar organoid formation, following the same protocol shown in Figure 3G. There was no difference in alveolar OFE between injury-exposed *Spp1*-/- AM co-cultures or control uninjured *Spp1*-/- AM co-cultures (Figure 4G-H). Although it is unlikely to be the sole *in* vivo factor driving AT2 proliferation after airway injury, these results suggest that OPN is one factor secreted by AMs that drives the AT2 cell proliferation response.

MANC2 lung mesenchyme responses to airway injury are dependent on alveolar macrophages

Because *Spp1*+ macrophages are associated with fibrosis in the lung and other organs[20,43], we further examined changes in the lung alveolar microenvironment after

airway injury. Other works have shown that macrophages and fibroblasts engage in cell-cell communication circuits that can regulate function and abundance of each cell type[44,45]. Although there was no large-scale remodeling of the murine lung after a single naphthalene injury (data not shown), changes in the mesenchyme could both support regeneration of the airway or serve as the basis for further dysregulation in the microenvironment. We performed scRNA-seq of FACS-enriched CD31-/CD45-/EpCAM-lung mesenchyme at days 2 and 7 after acute naphthalene airway injury to investigate any potential changes that could affect the lung mesenchyme and extracellular matrix (ECM) (Figure S1A). We removed a low quality/dying cluster of alvFibroblasts (data not shown, see methods), and we identified and annotated various cell types using markers in published datasets of the adult murine lung mesenchyme[17,46,47] (Figure 5A-C, Figure S5A) (Table S6).

Among the mesenchymal cell types we identified were *Pdgfrα*-expressing cells: alveolar fibroblasts (alvFibroblast), mesenchymal alveolar niche cells (MANC1), and a cluster we refer to herein as Mesenchymal Airway/Adventitial Niche Cell 2 (MANC2) (Figure 5D). *Pdgfrα*+ alveolar fibroblasts and MANC1 cells have been previously described to support alveolar epithelial function and proliferation[7,17,48,49]. MANC2 cells, although similar to MANC1 cells (Figure S5A), were a transcriptionally distinct population. Subsetting and reclustering of MANC1 and MANC2 cells highlighted markers that distinguish MANC1 and MANC2 cells (Figure 5E-H). *Gli1* was lowly expressed in many mesenchymal clusters, indicating MANC2 are not simply the *Gli1*+ cells[50] (Figures S5B). *Hhip*, a marker of peribronchiolar fibroblasts[51], was highly expressed by the Myofibroblast cluster, but not MANC2 (Figure S5A). Notably, MANC2 cells expressed markers of collagen-producing adventitial fibroblasts surrounding lung vasculature, such as *Adh7*, *Pi16*, *Dcn*, *and Hhip*[47] (Figure S5A). IF co-staining of the MANC2 cell marker Aqp1 in Pdgfra-CreERT2+/-;R26-LSL-Tomato+/- mice identified the presence of MANC2 cells underneath airway epithelium, as well as close to the vascular adventitia and in the alveolar space (Figure 5I). Furthermore, IF of the lineage label in tamoxifen-induced Lgr6-EGFP-CreERT2;R26-LSL-Tomato mice indicated the distinction between MANC2 cells and Lgr6+ airway smooth muscle cells[52] (Figure S5C-D).

We further characterized the MANC2 response to naphthalene treatment due to their unique location and response to airway injury. We identified upregulated DEGs in MANC2 cells at day 7 after injury compared to corn oil controls, a time point after the increase in AM abundance (Table S7). Upon GO Biological Process analysis and Reactome Pathway analysis of the DEGs, we observed a representation of terms and pathways associated with development, structure, and ECM (Figure S5E-F). Although a single naphthalene injury does not lead to detectable fibrosis in the lungs, these results indicate that airway injury alone causes MANC2 cells to upregulate pro-fibrotic transcriptional signatures in the alveolar space. Next, scRNA-seq suggested the MANC2 cells were present in increased proportions after airway injury as compared to control (Figure 5B-C). We developed a flow cytometry strategy to quantify MANC2 cells, which are Sca1- and CD34+, and confirmed the enrichment of MANC2 marker genes in the FACS-isolated CD31-/CD45-/EpCAM-/Sca1-/CD34+ fraction of mesenchymal cells via qPCR (Figure 5J, Figure S5G-I). MANC2 cells were increased in abundance at day 7 after naphthalene airway injury (Figure 5K). Upon AM depletion using clodronate liposome pre-treatment, the MANC2 cells failed to increase in abundance at day 7 after naphthalene injury (Figure 5L). These results suggest that injury-responsive AMs are important mediators of the MANC2 response after airway injury.

Discussion

In this study, we highlight the complexity of lung responses to a seemingly simple club cell depletion specific to airways. In response to acute airway loss of club cells, we found that alveolar macrophages (AMs) impart aberrant effects in the alveolar epithelium, specifically in the alveolar progenitor cells, AT2 cells. Our work also revealed alterations in mesenchymal cells we identified and termed Mesenchymal Airway/Adventitial Niche Cell 2 (MANC2) cells after airway injury. The transient dysregulation of AT2 progenitor cells after acute club cell injury highlights distal lung responses that could underlie more complex airway injuries/disease states, but also the lungs' propensity to restore homeostasis.

Our results demonstrate how damage to one epithelial compartment can elicit altered homeostasis in another compartment of the same tissue, making our findings distinct from other contexts in which macrophages have been implicated in lung epithelial cell responses. Macrophages promote airway epithelial proliferation at the site of club cell injury for repair[14], and our work illuminates how AMs can promote cell type-specific proliferative effects in distant, uninjured alveolar epithelium. AMs can positively regulate alveolar epithelial proliferation in the event of direct and pervasive lung alveolar damage after bleomycin injury, hookworm infection, and influenza[53,54], yet a distant alveolar epithelial proliferation response to an airway injury has not been described. In the pneumonectomy model, macrophages have a role in alveolar proliferation[12]. Notably, compensatory growth after pneumonectomy involves widespread proliferation of most cell types; in contrast, we found club cell ablation imparts effects in specific cell types such as AT2 cells and MANC2. We did not identify changes in AT1 cell abundance or AT1 cell proliferation, and we did not observe the appearance of cells marked by Krt8 after club cell airway ablation (data not shown). Thus, airway injury appears to cause changes in AMs and subsequent alteration in distant sites of the lung that are distinct from those associated with transitional alveolar cell states[27–29].

We identified *Spp1* upregulation in AMs after club cell injury, defining a functional role for *Spp1*/OPN, which has been associated with several injury or disease states without an appreciated reason. Of note, *Spp1* has been associated with fibrosis and cancer in the lungs and other organs such as the liver[6,20,43,55,56]. *Spp1*+ macrophages are suggested to play key roles in cancer of the breast, skin, brain, liver, and neck[56–59]. In lung cancers, *Spp1* is expressed by tumor-associated macrophages and is associated with poor prognosis[60]. Co-culture of AMs from naphthalene injured mice increased the OFE of AT2 cells compared to co-culture with AMs from uninjured mice. The failure of AMs from *Spp1-/-* naphthalene injured mice to stimulate increased alveolar OFE suggests that *Spp1*/OPN is necessary to promote additional alveolar organoid growth.

Further investigation of the effects of AMs in the lung revealed changes in a previously uncharacterized mesenchymal cell population, MANC2, during club cell airway injury.

Spp1+ macrophages are implicated in fibrotic lung disease, but their exact mechanism of cellular crosstalk is uncharacterized[6,43]. In this study, we identified an increase in MANC2 cells after club cell injury and a dependency on AMs for this response. Additionally, MANC2 cells upregulated pro-fibrotic transcriptional programs, despite an absence of fibrosis or massive tissue remodeling after a single club cell injury. Adventitial fibroblasts present in a scRNA-seq dataset in a previous report may be similar to MANC2 cells[47]. Consistent with this idea, we observed MANC2 cells underneath the airway epithelium and in the adventitia. How MANC2 cells uniquely contribute to the lung microenvironment during fibrotic disease and if they regulate specific epithelial populations such as AT2 cells and club cells remains to be studied.

Further understanding of the dual abilities of AMs in restoring and disrupting tissue homeostasis will be critical in designing potential therapies for lung diseases. AMs may be utilized or targeted in therapies for conditions associated with increased epithelial growth, such as lung cancer, and lung diseases associated with fibrosis, such as COVID-19 and idiopathic pulmonary fibrosis. Although the effects of alveolar macrophages we observed were resolved after a single acute airway injury, future studies could elucidate how these responses can intersect or become exacerbated with more severe, durable, or complex lung injuries and disease states. We hypothesize that MANC2-like cells and AMs stimulated by lung cell injury or infection have roles in human lung conditions that feature peribronchiolar fibrosis such as bronchiolitis obliterans syndrome and hypersensitivity pneumonitis associated with organic dusts or aerosols, occupational lung disease, and cigarette smoking[61,62]. Our work further underscores how the return to tissue homeostasis after an injury is a highly complex process, with effects that span the site of damage to areas that are undamaged. Building upon this knowledge will illuminate how lung diseases develop and how to design improved therapies for patients.

Acknowledgements

We thank Kim Lab members, Rania Dagher, Michal Shoskes-Carmel, Ramesh Shivdasani, Allon Klein, David Breault and Ke Yuan for thoughtful discussions on this

project. We thank Ronald Mathieu, Mahnaz Paktinat, and Ranjan Maskey of the BCH Flow Cytometry Core. We also thank Kevin Bi and Preetida Bhetariya for advising on scRNA-seq data analysis.

Funding

This work was supported in part by 1F31HL159919 (I.G.W.); Harvard College Research Program (JS); Damon Runyon Cancer Research Foundation Postdoctoral Fellowship (DRG:2368-19), Burroughs-Welcome Fund Postdoctoral Enrichment Program Award (1019903) (A.L.M.); 1F31HL172650 (A.B.V.); Landry Cancer Biology Research Fellowship (S.M.D.); 1R35GM150816 (R.A.F.), R01 HL090136, R01 HL132266, R01 HL125821, U01 HL100402 RFA-HL-09-004, R35HL150876, LONGFONDS | Accelerate, project BREATH, and the Harvard Stem Cell Institute (C.F.K.).

Data Availability

All raw and processed scRNA-seq data were deposited to the NCBI Gene Expression Omnibus (GEO) and Sequencing Read Archive (SRA). Bioinformatics analysis are uploaded on GitHub https://github.com/irwon/naphthalene. GEO data and bioinformatics analysis will be made publicly available upon publication of the peer-reviewed article.

Author Contributions

I.G.W. designed, conceived, and performed the experiments and wrote the manuscript. J.S., V.Y., A.B.V., S.D., A.S., M.J.R., designed and performed experiments, I.G.W. and A.M. generated and analyzed scRNA-seq data. R.B. performed histopathological analysis. S.M.J., S.P.R., M.P., R.A.F. and C.F.K supervised the design and study and co-wrote the manuscript. All authors reviewed and edited the manuscript.

Competing Interests

C.F.K. had a sponsored research agreement with Celgene/BMS Corporation during part of the period of these studies, yet the work in that agreement did not overlap with this study. C.F.K. and A.L.M. are founders of Cellforma. I.G.W. and all other authors declare no competing interests.

Figure Legends

Figure 1: Transient proliferation of AT2 cells after naphthalene airway injury.

A. Schematic of isolating lung epithelial cells from corn oil control mice or naphthalene-treated mice for scRNA-seq.
B. IF of corn oil control or naphthalene-treated mouse lungs. Blue = DAPI, Yellow = SPC, Magenta = Acetylated tubulin, White = CCSP. Scale bar = 100 µm.
C. Merged UMAP plot of epithelial cells from (A). N = 3 mice per condition. Corn oil N = 10247 cells; Day 2 naphthalene N = 6886 cells; Day 7 Naphthalene N = 16857 cells. Abbreviations: Diff Club = Differentiating Club.
D. Split of the UMAP plot from (C) based on condition.
E. Proliferation score of merged lung epithelium scRNA-seq as shown in Figure 1B.
F. Subset of alveolar epithelial cells from (C).
G. Cluster fractions of (F). Boxes highly Proliferative AT2 cells.
H. IF images of corn oil control mice and naphthalene-treated mice sacrificed at indicated timepoints. Blue = DAPI, Yellow = SPC, Magenta = Ki67, White = CCSP. AW = airway. Scale bar = 100 µm.
I. Quantification of proliferative AT2 cells (Ki67+/SPC+) normalized to total AT2 cells at the indicated timepoints after naphthalene injury. Analysis was confined to fields that included an airway or terminal bronchiole. Data are represented as mean ± SEM. Corn oil N = 11 mice, Day 2 N = 4 mice, Day 7 N = 7 mice, Day 10 N = 6 mice. Day 14 N = 3 mice. Student's T-test: * = $p < 0.05$; *** = $p < 0.001$. **** = $p < 0.0001$. Absence of asterisk = no significance compared to control.
J. Quantification of proliferative AT2 cells (Ki67+/SPC+) normalized to total AT2 cells at the indicated timepoints after naphthalene injury. Analysis was confined to fields of alveolar space. Data are represented as mean ± SEM. Corn oil N = 9 mice, Day 2 N = 4 mice, Day 7 N = 7 mice, Day 10 N = 6 mice. Day 14 N = 3 mice. Student's T-test: * = $p < 0.05$; *** = $p < 0.001$. **** = $p < 0.0001$. Absence of asterisk = no significance compared to control.

See also Figure S1, Supplementary Tables 1-4.

Figure 2: Transient proliferation of AT2 cells after genetic club cell ablation.

A. Schematic of induction and injury of CCSP-CreER+/-; Rosa26-LSL-YFP/iDTR mice. PBS or DTA were administered via intratracheal injection.
B. IF images of mouse lungs at the indicated timepoints after genetic club cell ablation. Blue = DAPI, Yellow = SPC, Magenta = CCSP, Green = YFP. Scale bar = 100 µm.
C. Quantification of CCSP+ club cell loss in airways of CCSP-CreER+/-; Rosa26-LSL-YFP/iDTR mice after no intratracheal administration, PBS, or DTA administration at the indicated timepoints. Data are represented as mean ± SEM. N = 3-4 mice per condition, per timepoint. Student's T-test: *** = $p < 0.001$; ns = no significance.
D. IF images of PBS control mice and DTA-treated mice sacrificed at day 7 after injury. Blue = DAPI, Yellow = SPC, Magenta = Ki67, White = CCSP. AW = airway. Scale bar = 100 µm.
E. Quantification of proliferative AT2 cells (Ki67+/SPC+) normalized to total AT2 cells at the indicated timepoints after genetic club cell injury. Analysis was confined to fields of alveolar space. Data are represented as mean ± SEM. N = 3-5 mice per condition, per timepoint. Student's T-test: * = $p < 0.05$; ** = $p < 0.01$; ns = no significance.
F. Schematic of isolating alveolar-enriched Sca1- lung epithelial cells from corn oil control or naphthalene-treated mice.
G. IF of alveolar organoid co-cultures grown from Sca1- lung epithelium as diagrammed in (A). Blue = DAPI, Yellow = SPC, Magenta = RAGE. Scale bar = 1 mm.
H. Quantification of organoid forming efficiency of Sca1- alveolar organoids shown in (B). Data are represented as mean ± SEM. N = 5 mice per condition, per timepoint. Student's T-test: ns = no significance.

See also Figure S2.

Figure 3: Alveolar macrophages mediate AT2 cell proliferation after airway injury.

A. Flow cytometry strategy used to quantify macrophages from corn oil control or naphthalene-injured animals. CD11b+/Ly6G+ neutrophils were excluded from the CD45+ immune parental population before measuring the abundance of CD64+ total macrophages and delineating SiglecF+/CD11b- alveolar macrophages (AMs) from SiglecF-/CD11b+ interstitial macrophages (IMs). Monocytes may also appear in injury states within the SiglecF-/CD11b+ population, hence the additional annotation for naphthalene-treated animals.
B. Flow cytometry quantification of AMs and IMs/monocytes at the indicated timepoints after control or injury. Data are represented as mean ± SEM. N = 3-6 mice per condition, per timepoint. Student's T-test: * = $p < 0.05$; ns = no significance.
C. Schematic of liposome administration in mice prior to control or naphthalene injury. PBS control or clodronate liposome was administered daily via intratracheal injection.
D. Flow cytometry quantification of SiglecF+/Cd11B- AMs in liposome pre-treated animals with and without naphthalene injury, following the same gating strategy as show in (A). Data are represented as mean ± SEM. N = 3-6 mice per condition, per timepoint. Student's T-test: ** = $p < 0.01$; *** = $p < 0.001$.
E. IF of mice that received liposome pre-treatment prior to control or naphthalene injury, sacrificed at day 7 post-injury. Blue = DAPI, Yellow = SPC, Magenta = Ki67. Scale bar = 100 µm.
F. Quantification of proliferative AT2 cells (Ki67+/SPC+) normalized to total AT2 cells at day 7 (D7) after liposome pre-treatment and naphthalene injury. Analysis was confined to fields of alveolar space, as indicated. Data are represented as mean ± SEM. N = 5-6 mice per condition. Student's T-test: ** = $p < 0.01$; ns = no significance.
G. Schematic of isolating AMs from BAL fluid using CD45-positive selection with MACS. These AMs were combined with Sca1- alveolar-enriched epithelium from naïve DsRed animals.

H. IF of AM and alveolar epithelial organoid co-cultures. AMs were harvested from corn oil- or naphthalene-treated mice as shown in (H). Magenta = DsRed, Yellow = SPC. Scale bar = 1 mm.
I. Quantification of organoid forming efficiency of alveolar organoids shown in (I). Data are represented as mean ± SEM. N = 3 mice per condition. Student's T-test: ** = $p < 0.001$.

See also Figure S3.

Figure 4: Alveolar macrophages upregulate *Spp1* during airway repair.

A. Schematic of isolating AMs (via BAL) and remaining CD45+ immune cells from mice treated with corn oil control or naphthalene for scRNA-seq.
B. Merged UMAP plot of immune cells from (D). N = 3 mice per condition. Corn oil N = 7640 cells; Day 2 naphthalene N = 4102 cells; Day 7 Naphthalene N = 11888 cells.
C. Split of the UMAP plot from (B) based on condition.
D. Top 20 DEGs upregulated by AMs at day 7 after naphthalene injury, some of which are potential signaling molecules.
E. Expression of *Spp1* in scRNA-seq data.
F. Concentration of Osteopontin (OPN) in media of AM and alveolar organoid co-cultures from Figure 3H-J. Media was harvested at day 3 of co-culture prior to the first media change. Data are represented as mean ± SEM. Student's T-test: * = $p < 0.05$.
G. IF of *Spp1*-/- AM and alveolar epithelial organoid co-cultures. AMs were harvested from corn oil- or naphthalene-treated *Spp1*-/- mice, following a similar isolation strategy shown in Fig. 3G. Magenta = DsRed, Yellow = SPC. Scale bar = 1 mm.
H. Quantification of organoid forming efficiency of alveolar organoids shown in (H). Data are represented as mean ± SEM. N = 3 mice per condition. Student's T-test: ns = not significant.

See also Figure S4 and Supplementary Table S5.

Figure 5: MANC2 lung mesenchyme responses to airway injury are dependent on alveolar macrophages.

A. Merged UMAP plot of mesenchymal cells isolated from corn oil control and day 2 and 7 naphthalene-treated mice. FACS strategy to isolate mesenchyme is shown in Fig. S1B. Abbreviations: alvFibroblast = Alveolar Fibrobolast, MANC1 = Mesenchymal alveolar niche cell 1, MANC2 = Mesenchymal alveolar/airway niche cell 2, aSMC = Airway smooth muscle cell, vSMC = Vascular smooth muscle cell. N = 3 mice per condition. Corn oil N = 11589 cells; Day 2 naphthalene N = 6551 cells; Day 7 Naphthalene N = 14639 cells.
B. Split of the UMAP plot from (A) based on condition.
C. Cluster fractions of (A). Boxes highlight MANC2 cells.
D. *Pdgfra* expression in the merged mesenchyme from control and naphthalene-treated animals.
E. Subset and reclustering of MANC1 and MANC2 cells from (A).
F. Scoring of the MANC2 signature across the MANC subset, using the top 50 markers of MANC2 cells that distinguish them from the other cell clusters in (E).
G. Gene expression of MANC1 markers in the MANC subset from (E).
H. Gene expression of MANC2 markers in the MANC subset from (E).
I. IF of Aqp1+ MANC2 cells in lineage-labelled PdgfraCreERT2+/-;R26-tdTomato/+ mice that were uninjured (corn oil) or treated with naphthalene. Blue = DAPI, Yellow = Aqp1; Magenta = Pdgfra Tomato lineage label. Scale bar = 50 µm.
J. Flow cytometry strategy used to examine Sca1-/CD34+ MANC2 cells.
K. Flow cytometry quantification using the gating strategy shown in (J) of Sca1-/CD34+ MANC2 cells after naphthalene injury. Animals were sacrificed at the indicated timepoints. Corn oil controls were normalized to 1 (dotted line), and Sca1-/CD34+ mesenchyme abundance in injured animals was normalized to the respective controls at each timepoint. Data are represented as mean ± SEM. Student's T-test: * = $p < 0.05$; ns = no significance.
L. Flow cytometry quantification using the gating strategy shown in (J) of Sca1-/CD34+ MANC2 lung mesenchymal cells in mice pre-treated with PBS control or clodronate liposomes, followed by corn oil control or naphthalene injury. Mice

were sacrificed at day 7 after the naphthalene injury. PBS liposome-corn oil controls were normalized to 1 (dotted line), and Sca1-/CD34+ mesenchyme abundance across the remaining conditions were normalized to the PBS liposome-corn oil control. Data are represented as mean ± SEM. Student's T-test: ** = $p < 0.01$; ns = no significance.

See also Figure S5 and Supplementary Table S7.

Methods

Mice

Adult mice (8-12 weeks) were used for all studies. C57Bl/6J mice (Jackson Laboratory) were utilized unless otherwise noted. CCSP-CreER (Jackson Laboratory #016225) mice were crossed to R26-LSL-YFP (Jackson Laboratory #006148) and maintained at homozygosity for both genes. CCSP-CreER; R26-LSL-YFP were then crossed to homozygous R26-LSL-iDTR (Jackson Laboratory #007900) mice to create CCSP-CreER+/-; R26-LSL-YFP/iDTR mice for genetic club cell ablation and club cell lineage tracing studies. Lgr6-EGFP-CreERT2;R26-LSL-Tomato mice were bred, induced, and harvested as described previously[52]. *Spp1*KO mice were obtained from the Jackson Laboratory (Stock #004936). All mice were maintained in virus-free conditions and housed in groups, and all experiments were approved by the Boston Children's Hospital Animal Care and Use Committee. Due to documented sex differences in the response to naphthalene-mediated club cell injury[63], female mice were utilized for injury studies and grouped by litter when possible.

Naphthalene Injury

Naphthalene (Sigma Adrich #84679) was dissolved in corn oil at a concentration of 20 mg/mL at room temperature and sterile filtered before administration. C57Bl/6J or CCSP-CreER+/-; R26-LSL-YFP/iDTR mice were injected intraperitoneally with naphthalene at 200 mg/kg body weight or an equivalent volume of corn oil for control animals. Mice were then monitored for signs of distress throughout recovery until sacrificed with anesthetic overdose at indicated timepoints.

Genetic club cell ablation

CCSP-CreER+/-; R26-LSL-YFP/iDTR were first induced by 4 intraperitoneal injections of tamoxifen (Sigma Aldrich T5648) administered once daily, at 100 mg/kg body weight (stock solution 20 mg/mL in corn oil). On the third day after the last dose of tamoxifen, diphtheria toxin (Sigma Aldrich D0564) was administered via intratracheal injection at 3 µg/kg body weight (stock solution 60 µg/mL in PBS) or PBS control. Mice were then monitored for signs of distress throughout recovery and sacrificed at indicated timepoints.

Lung tissue preparation, flow cytometry, FACS

Lungs were dissected, prepared, stained, analyzed, and sorted as described previously[21]. For experiments that required the retention of a lung lobe for histology in addition to tissue processing for flow cytometry, the left lobe was isolated and removed using a hemostat. Flow cytometry analysis was performed on a BD LSR II or LSR Fortessa, and experiments that required sorting utilized a BD FACSAria II. Analysis of all samples was performed using BD FACSDiva software.

For flow cytometry and sorting experiments of immune cell populations, BAL (see below for method) recovery of AMs was performed and later combined with digested, single cell lung suspensions. Samples were then blocked with anti-mouse CD16/32 antibody (BioLegend #101302) for 5 minutes on ice prior to cell surface staining.

Bronchoalveolar lavage (BAL)

Mice were euthanized by anesthetic overdose (avertin) and a 22G Safelet catheter was affixed through the trachea using surgical suture. BAL fluid was obtained from animals by injecting and withdrawing 1 mL of warm 2% FBS, 2mM EDTA PBS solution (37°C), through the catheter, and repeated up to 3 times. BAL fluid was then stored on ice until its use in flow cytometry, scRNA-seq, or MACS.

Macrophage depletion

Female C57/Bl6J mice were first anesthetized with isoflurane and sterile liposomes containing PBS or clodronate (Liposoma BV #CP-005-005) were administered to animals via intratracheal administration at 50 uL per 20 g animal. Mice were given daily doses over 4 days. Naphthalene injury was performed 3 days after the last dose of liposomes, as described above.

Lung organoid co-cultures

AT2 cells were obtained via FACS (CD31-/CD45-/Ter119-/EpCAM+/Sca1-) from uninjured control or injured C57 Bl/6 and grown in co-culture conditions with stromal cells as previously described[32]. For co-culture conditions with alveolar macrophages, naïve DsRed mice were used as the source of AT2 cells (CD31-/CD45-/Ter119-/EpCAM+/Sca1-) while control or injured C57 Bl/6 mice were used as the source of AMs. AM co-cultures used media described in Konishi et al.[37] and omitted IL-1β and EGF.

MACS enrichment of alveolar macrophages

BAL fluid was collected from uninjured control or injured animals as described and red blood cells were lysed (0.154M NH_4Cl/10mM $KHCO_3$/0.127mM EDTA). The remaining cell suspension was incubated with CD45 magnetic beads (Miltenyi #130-052-301) and positively selected using the OctoMACS (Miltenyi) platform. Cells were then passed through a 0.4µm cell strainer prior to lung organoid co-culture.

Histology and immunostaining

For histology of the lungs, mouse lung tissues were perfused, inflated with 0.8% low melting agarose in PBS, and fixed overnight at 4°C in 10% neutral-buffered formalin. Tissues were then switched to 70% ethanol prior to paraffin embedding. Formalin-fixed, paraffin embedded lung sections were cut to 5 µm thickness and mounted onto glass slides. Hematoxylin and eosin or Masson's trichrome staining was performed where indicated. For immunofluorescence experiments, slides were de-waxed and antigen retrieval was performed with citrate buffer (pH6, Vector Laboratories H-3300).

Measurement of OPN concentration in AM organoid co-cultures

Media was harvested from AM organoid co-cultures at 3 days of culture before the first media change and stored at -20º C. ELISA was performed using the Mouse/Rat Osteopontin (OPN) Quantikine ELISA Kit (R&D Systems) following the manufacturers protocol.

qPCR of MANC2 or mesothelium markers

RNA was extracted from sorted populations using the Absolutely RNA Microprep Kit (Agilent Technologies #400805). cDNA was created using the High-Capacity cDNA Reverse Transcription Kit with RNAse Inhibitor (Applied Biosystems #4374966). qPCR was performed using the Taqman Gene Expression Assays platform with the following probes: Adh7 Mm00507750_m1, Aqp1 Mm01326466_m1, Bmp7 Mm00432102_m1, Dner Mm00548872_m1, Lamc3 Mm01324510_m1, Nbl1 Mm00500746_m1, Msln Mm00450770_m1, Slpi Mm00441530_g1, Upk3b Mm00558406_m1. Housekeeping gene probe: Rn18s Mm03928990_g1.

Generation and analysis of scRNA-seq data

Mouse epithelial and mesenchymal cell preparation

Female adult C57/Bl6J mice were injured with naphthalene or given control injections as described above and sacrificed at days 2 or 7 after injury. Epithelial populations were isolated from the CD31-/CD45-/EpCAM+/Sca1- and CD31-/CD45-/EpCAM+/Sca1+ gates by FACS (n = 3 mice per condition). Mesenchymal cells were sorted from the CD31-/CD45-/EpCAM- gate by FACS (n=3 mice per condition) using the same animals.

Mouse immune cell preparation

Female adult C57/Bl6J mice were injured with naphthalene or given control injections as described above and sacrificed at days 2 or 7 after injury. Before extracting lungs from the animals, BAL fluid was obtained from the mice as described above and set aside on ice. The remaining lung tissue was dissociated and stained, and immune cells were isolated by FACS based on CD31-/CD119-/CD45+ surface markers. For sequencing,

BAL fluid was combined with sorted immune cells at a 1:1 ratio per animal (n=3 mice per condition).

Library preparation

ScRNA-seq was performed using the 10x Genomics platform. Cells were encapsulated with a 10X Genomics Chromium Controller Instrument and the following reverse transcription, cDNA amplification, and library preparation were performed using the Chromium Next GEM Single Cell 2' v3 or v3.1 kits. Quantification and quality control of cDNA was determined using a QubitTM dsDNA HS assay kit and the Agilent TapeStation High Sensitivity D5000 ScreenTape System. Libraries were sequenced using an Illumina NextSeq500 at a depth of ~50,000 reads/cell and later processed using CellRanger.

Analysis of scRNA-seq data

Analysis of raw CellRanger data was performed using Seurat v3. Cells were filtered for UMI ≥ 500, genes ≥ 300, mitochondrial DNA ratio < 0.2, and log10 genes per UMI > 0.80. After filtering and clustering of the epithelial scRNA-seq data, we removed the AT2 stressed cluster (Figure S1C) due to the high expression of mitochondrial DNA and lncRNAs associated with ribosomal RNA contamination[64,65]. We additionally removed an alvFibroblast2 cluster (data not shown) from the mesenchymal scRNA-seq data for similar reasons. The remaining epithelial or mesenchymal cells were re-clustered in their respective datasets and used for downstream analysis (Figure 1B). For the epithelial, immune, and mesenchymal scRNA-seq, differential gene expression analysis was performed with Seurat "FindMarkers" function to identify positively upregulated genes with a log fold change > 0.25. Proliferation score was calculated using "AddModuleScore" with the genes Pbk, Birc5, Mki6, Ube2c, Top2a, Tk1, Aurkb, Cdkn3, Cenpf, Cdk1, Zwint. Gene Ontology and Reactome Pathway analysis was performed using Panther 18.0[41].

References

1. Butler, J.P., Loring, S.H., Patz, S., Tsuda, A., Yablonskiy, D.A., and Mentzer, S.J. (2012). Evidence for adult lung growth in humans. N. Engl. J. Med. *367*, 244–247.

2. Mentzer, S.J. (2018). The puzzling mechanism of compensatory lung growth. Stem Cell Investig *5*, 8.

3. Sun, F., and Poss, K.D. (2023). Inter-organ communication during tissue regeneration. Development *150*. 10.1242/dev.202166.

4. Rodgers, J.T., King, K.Y., Brett, J.O., Cromie, M.J., Charville, G.W., Maguire, K.K., Brunson, C., Mastey, N., Liu, L., Tsai, C.-R., et al. (2014). mTORC1 controls the adaptive transition of quiescent stem cells from G0 to G(Alert). Nature *510*, 393–396.

5. Johnson, K., Bateman, J., DiTommaso, T., Wong, A.Y., and Whited, J.L. (2018). Systemic cell cycle activation is induced following complex tissue injury in axolotl. Dev. Biol. *433*, 461–472.

6. Sikkema, L., Ramírez-Suástegui, C., Strobl, D.C., Gillett, T.E., Zappia, L., Madissoon, E., Markov, N.S., Zaragosi, L.-E., Ji, Y., Ansari, M., et al. (2023). An integrated cell atlas of the lung in health and disease. Nat. Med., 1–15.

7. Barkauskas, C.E., Cronce, M.J., Rackley, C.R., Bowie, E.J., Keene, D.R., Stripp, B.R., Randell, S.H., Noble, P.W., and Hogan, B.L.M. (2013). Type 2 alveolar cells are stem cells in adult lung. J. Clin. Invest. *123*, 3025–3036.

8. Rawlins, E.L., Ostrowski, L.E., Randell, S.H., and Hogan, B.L.M. (2007). Lung development and repair: contribution of the ciliated lineage. Proc. Natl. Acad. Sci. U. S. A. *104*, 410–417.

9. Whitsett, J.A. (2018). Airway Epithelial Differentiation and Mucociliary Clearance. Ann. Am. Thorac. Soc. *15*, S143–S148.

10. Guha, A., Deshpande, A., Jain, A., Sebastiani, P., and Cardoso, W.V. (2017). Uroplakin 3a+ Cells Are a Distinctive Population of Epithelial Progenitors that Contribute to Airway Maintenance and Post-injury Repair. Cell Rep. *19*, 246–254.

11. Basil, M.C., Katzen, J., Engler, A.E., Guo, M., Herriges, M.J., Kathiriya, J.J., Windmueller, R., Ysasi, A.B., Zacharias, W.J., Chapman, H.A., et al. (2020). The Cellular and Physiological Basis for Lung Repair and Regeneration: Past, Present, and Future. Cell Stem Cell *26*, 482–502.

12. Lechner, A.J., Driver, I.H., Lee, J., Conroy, C.M., Nagle, A., Locksley, R.M., and Rock, J.R. (2017). Recruited Monocytes and Type 2 Immunity Promote Lung Regeneration following Pneumonectomy. Cell Stem Cell *21*, 120-134.e7.

13. Engler, A.E., Ysasi, A.B., Pihl, R.M.F., Villacorta-Martin, C., Heston, H.M., Richardson, H.M.K., Thapa, B.R., Moniz, N.R., Belkina, A.C., Mazzilli, S.A., et al. (2020). Airway-Associated Macrophages in Homeostasis and Repair. Cell Rep. *33*, 108553.

14. Dagher, R., Copenhaver, A.M., Besnard, V., Berlin, A., Hamidi, F., Maret, M., Wang, J., Qu, X., Shrestha, Y., Wu, J., et al. (2020). IL-33-ST2 axis regulates myeloid cell differentiation and activation enabling effective club cell regeneration. Nat. Commun. *11*, 4786.

15. Reyes, N.S., Krasilnikov, M., Allen, N.C., Lee, J.Y., Hyams, B., Zhou, M., Ravishankar, S., Cassandras, M., Wang, C., Khan, I., et al. (2022). Sentinel *p16*$^{INK4a+}$ cells in the basement membrane form a reparative niche in the lung. Science *378*, 192–201.

16. Li, R., Bernau, K., Sandbo, N., Gu, J., Preissl, S., and Sun, X. (2018). Pdgfra marks a cellular lineage with distinct contributions to myofibroblasts in lung maturation and injury response. Elife *7*. 10.7554/eLife.36865.

17. Zepp, J.A., Zacharias, W.J., Frank, D.B., Cavanaugh, C.A., Zhou, S., Morley, M.P., and Morrisey, E.E. (2017). Distinct Mesenchymal Lineages and Niches Promote Epithelial Self-Renewal and Myofibrogenesis in the Lung. Cell *170*, 1134-1148.e10.

18. Perl, A.-K.T., Riethmacher, D., and Whitsett, J.A. (2011). Conditional depletion of airway progenitor cells induces peribronchiolar fibrosis. Am. J. Respir. Crit. Care Med. *183*, 511–521.

19. Aoshiba, K., Tsuji, T., Itoh, M., Semba, S., Yamaguchi, K., Nakamura, H., and Watanabe, H. (2014). A murine model of airway fibrosis induced by repeated naphthalene exposure. Exp. Toxicol. Pathol. *66*, 169–177.

20. Ouyang, J.F., Mishra, K., Xie, Y., Park, H., Huang, K.Y., Petretto, E., and Behmoaras, J. (2023). Systems level identification of a matrisome-associated macrophage polarisation state in multi-organ fibrosis. Elife *12*. 10.7554/eLife.85530.

21. Louie, S.M., Moye, A.L., Wong, I.G., Lu, E., Shehaj, A., Garcia-de-Alba, C., Ararat, E., Raby, B.A., Lu, B., Paschini, M., et al. (2022). Progenitor potential of lung epithelial organoid cells in a transplantation model. Cell Rep. *39*, 110662.

22. Volckaert, T., Dill, E., Campbell, A., Tiozzo, C., Majka, S., Bellusci, S., and De Langhe, S.P. (2011). Parabronchial smooth muscle constitutes an airway epithelial stem cell niche in the mouse lung after injury. J. Clin. Invest. *121*, 4409–4419.

23. Buckpitt, A., Boland, B., Isbell, M., Morin, D., Shultz, M., Baldwin, R., Chan, K., Karlsson, A., Lin, C., Taff, A., et al. (2002). Naphthalene-induced respiratory tract toxicity: metabolic mechanisms of toxicity. Drug Metab. Rev. *34*, 791–820.

24. Buckpitt, A., Kephalopoulos, S., Koistinen, K., Kotzias, D., Morawska, L., and Sagunski, H. (2010). Naphthalene (World Health Organization).

25. Gerdes, J., Lemke, H., Baisch, H., Wacker, H.H., Schwab, U., and Stein, H. (1984). Cell cycle analysis of a cell proliferation-associated human nuclear antigen defined by the monoclonal antibody Ki-67. J. Immunol. *133*, 1710–1715.

26. Giangreco, A., Reynolds, S.D., and Stripp, B.R. (2002). Terminal bronchioles harbor a unique airway stem cell population that localizes to the bronchoalveolar duct junction. Am. J. Pathol. *161*, 173–182.

27. Choi, J., Park, J.-E., Tsagkogeorga, G., Yanagita, M., Koo, B.-K., Han, N., and Lee, J.-H. (2020). Inflammatory Signals Induce AT2 Cell-Derived Damage-Associated Transient Progenitors that Mediate Alveolar Regeneration. Cell Stem Cell *27*, 366-382.e7.

28. Strunz, M., Simon, L.M., Ansari, M., Kathiriya, J.J., Angelidis, I., Mayr, C.H., Tsidiridis, G., Lange, M., Mattner, L.F., Yee, M., et al. (2020). Alveolar regeneration through a Krt8+ transitional stem cell state that persists in human lung fibrosis. Nat. Commun. *11*, 3559.

29. Kobayashi, Y., Tata, A., Konkimalla, A., Katsura, H., Lee, R.F., Ou, J., Banovich, N.E., Kropski, J.A., and Tata, P.R. (2020). Persistence of a regeneration-associated, transitional alveolar epithelial cell state in pulmonary fibrosis. Nat. Cell Biol. *22*, 934–946.

30. Buch, T., Heppner, F.L., Tertilt, C., Heinen, T.J.A.J., Kremer, M., Wunderlich, F.T., Jung, S., and Waisman, A. (2005). A Cre-inducible diphtheria toxin receptor mediates cell lineage ablation after toxin administration. Nat. Methods *2*, 419–426.

31. Rawlins, E.L., Okubo, T., Xue, Y., Brass, D.M., Auten, R.L., Hasegawa, H., Wang, F., and Hogan, B.L.M. (2009). The role of Scgb1a1+ Clara cells in the long-term maintenance and repair of lung airway, but not alveolar, epithelium. Cell Stem Cell *4*, 525–534.

32. Lee, J.-H., Bhang, D.H., Beede, A., Huang, T.L., Stripp, B.R., Bloch, K.D., Wagers, A.J., Tseng, Y.-H., Ryeom, S., and Kim, C.F. (2014). Lung stem cell differentiation in mice directed by endothelial cells via a BMP4-NFATc1-thrombospondin-1 axis. Cell *156*, 440–455.

33. Rodríguez-Morales, P., and Franklin, R.A. (2023). Macrophage phenotypes and functions: resolving inflammation and restoring homeostasis. Trends Immunol. 10.1016/j.it.2023.10.004.

34. Thepen, T., Van Rooijen, N., and Kraal, G. (1989). Alveolar macrophage elimination in vivo is associated with an increase in pulmonary immune response in mice. J. Exp. Med. *170*, 499–509.

35. Van Rooijen, N., and Sanders, A. (1994). Liposome mediated depletion of macrophages: mechanism of action, preparation of liposomes and applications. J. Immunol. Methods *174*, 83–93.

36. Van Hoecke, L., Job, E.R., Saelens, X., and Roose, K. (2017). Bronchoalveolar Lavage of Murine Lungs to Analyze Inflammatory Cell Infiltration. J. Vis. Exp. 10.3791/55398.

37. Konishi, S., Tata, A., and Tata, P.R. (2022). Defined conditions for long-term expansion of murine and human alveolar epithelial stem cells in three-dimensional cultures. STAR Protoc *3*, 101447.

38. Franzén, O., Gan, L.-M., and Björkegren, J.L.M. (2019). PanglaoDB: a web server for exploration of mouse and human single-cell RNA sequencing data. Database *2019*. 10.1093/database/baz046.

39. Lee, J.S., Koh, J.-Y., Yi, K., Kim, Y.-I., Park, S.-J., Kim, E.-H., Kim, S.-M., Park, S.H., Ju, Y.S., Choi, Y.K., et al. (2021). Single-cell transcriptome of bronchoalveolar lavage fluid reveals sequential change of macrophages during SARS-CoV-2 infection in ferrets. Nat. Commun. *12*, 4567.

40. Wang, L., Netto, K.G., Zhou, L., Liu, X., Wang, M., Zhang, G., Foster, P.S., Li, F., and Yang, M. (2021). Single-cell transcriptomic analysis reveals the immune landscape of lung in steroid-resistant asthma exacerbation. Proc. Natl. Acad. Sci. U. S. A. *118*. 10.1073/pnas.2005590118.

41. Thomas, P.D., Ebert, D., Muruganujan, A., Mushayahama, T., Albou, L.-P., and Mi, H. (2022). PANTHER: Making genome-scale phylogenetics accessible to all. Protein Sci. *31*, 8–22.

42. Liaw, L., Birk, D.E., Ballas, C.B., Whitsitt, J.S., Davidson, J.M., and Hogan, B.L. (1998). Altered wound healing in mice lacking a functional osteopontin gene (spp1). J. Clin. Invest. *101*, 1468–1478.

43. Morse, C., Tabib, T., Sembrat, J., Buschur, K.L., Bittar, H.T., Valenzi, E., Jiang, Y., Kass, D.J., Gibson, K., Chen, W., et al. (2019). Proliferating SPP1/MERTK-expressing macrophages in idiopathic pulmonary fibrosis. Eur. Respir. J. *54*. 10.1183/13993003.02441-2018.

44. Zhou, X., Franklin, R.A., Adler, M., Jacox, J.B., Bailis, W., Shyer, J.A., Flavell, R.A., Mayo, A., Alon, U., and Medzhitov, R. (2018). Circuit Design Features of a Stable Two-Cell System. Cell *172*, 744-757.e17.

45. Zhou, X., Franklin, R.A., Adler, M., Carter, T.S., Condiff, E., Adams, T.S., Pope, S.D., Philip, N.H., Meizlish, M.L., Kaminski, N., et al. (2022). Microenvironmental sensing by fibroblasts controls macrophage population size. Proc. Natl. Acad. Sci. U. S. A. *119*, e2205360119.

46. Xie, T., Wang, Y., Deng, N., Huang, G., Taghavifar, F., Geng, Y., Liu, N., Kulur, V., Yao, C., Chen, P., et al. (2018). Single-Cell Deconvolution of Fibroblast Heterogeneity in Mouse Pulmonary Fibrosis. Cell Rep. *22*, 3625–3640.

47. Tsukui, T., Sun, K.-H., Wetter, J.B., Wilson-Kanamori, J.R., Hazelwood, L.A., Henderson, N.C., Adams, T.S., Schupp, J.C., Poli, S.D., Rosas, I.O., et al. (2020). Collagen-producing lung cell atlas identifies multiple subsets with distinct localization and relevance to fibrosis. Nat. Commun. *11*, 1920.

48. Green, J., Endale, M., Auer, H., and Perl, A.-K.T. (2016). Diversity of Interstitial Lung Fibroblasts Is Regulated by Platelet-Derived Growth Factor Receptor α Kinase Activity. Am. J. Respir. Cell Mol. Biol. *54*, 532–545.

49. Chung, M.-I., Bujnis, M., Barkauskas, C.E., Kobayashi, Y., and Hogan, B.L.M. (2018). Niche-mediated BMP/SMAD signaling regulates lung alveolar stem cell proliferation and differentiation. Development *145*. 10.1242/dev.163014.

50. Cassandras, M., Wang, C., Kathiriya, J., Tsukui, T., Matatia, P., Matthay, M., Wolters, P., Molofsky, A., Sheppard, D., Chapman, H., et al. (2020). Gli1+ mesenchymal stromal cells form a pathological niche to promote airway progenitor metaplasia in the fibrotic lung. Nat. Cell Biol. *22*, 1295–1306.

51. Wang, C., Hyams, B., Allen, N.C., Cautivo, K., Monahan, K., Zhou, M., Dahlgren, M.W., Lizama, C.O., Matthay, M., Wolters, P., et al. (2023). Dysregulated lung stroma drives emphysema exacerbation by potentiating resident lymphocytes to suppress an epithelial stem cell reservoir. Immunity *56*, 576-591.e10.

52. Lee, J.-H., Tammela, T., Hofree, M., Choi, J., Marjanovic, N.D., Han, S., Canner, D., Wu, K., Paschini, M., Bhang, D.H., et al. (2017). Anatomically and Functionally Distinct Lung Mesenchymal Populations Marked by Lgr5 and Lgr6. Cell *170*, 1149-1163.e12.

53. Hung, L.-Y., Sen, D., Oniskey, T.K., Katzen, J., Cohen, N.A., Vaughan, A.E., Nieves, W., Urisman, A., Beers, M.F., Krummel, M.F., et al. (2019). Macrophages promote epithelial proliferation following infectious and non-infectious lung injury through a Trefoil factor 2-dependent mechanism. Mucosal Immunol. *12*, 64–76.

54. Pervizaj-Oruqaj, L., Selvakumar, B., Ferrero, M.R., Heiner, M., Malainou, C., Glaser, R.D., Wilhelm, J., Bartkuhn, M., Weiss, A., Alexopoulos, I., et al. (2024). Alveolar macrophage-expressed Plet1 is a driver of lung epithelial repair after viral pneumonia. Nat. Commun. *15*, 87.

55. Kumar, A., Elko, E., Bruno, S.R., Mark, Z.F., Chamberlain, N., Mihavics, B.K., Chandrasekaran, R., Walzer, J., Ruban, M., Gold, C., et al. (2022). Inhibition of PDIA3 in club cells attenuates osteopontin production and lung fibrosis. Thorax *77*, 669–678.

56. Bill, R., Wirapati, P., Messemaker, M., Roh, W., Zitti, B., Duval, F., Kiss, M., Park, J.C., Saal, T.M., Hoelzl, J., et al. (2023). CXCL9:SPP1 macrophage polarity identifies a network of cellular programs that control human cancers. Science *381*, 515–524.

57. Zhao, H., Chen, Q., Alam, A., Cui, J., Suen, K.C., Soo, A.P., Eguchi, S., Gu, J., and Ma, D. (2018). The role of osteopontin in the progression of solid organ tumour. Cell Death Dis. *9*, 356.

58. Wang, J.-B., Zhang, Z., Li, J.-N., Yang, T., Du, S., Cao, R.-J., and Cui, S.-S. (2020). SPP1 promotes Schwann cell proliferation and survival through PKCα by binding with CD44 and αvβ3 after peripheral nerve injury. Cell Biosci. *10*, 98.

59. Tan, Y., Zhao, L., Yang, Y.-G., and Liu, W. (2022). The Role of Osteopontin in Tumor Progression Through Tumor-Associated Macrophages. Front. Oncol. *12*, 953283.

60. Matsubara, E., Yano, H., Pan, C., Komohara, Y., Fujiwara, Y., Zhao, S., Shinchi, Y., Kurotaki, D., and Suzuki, M. (2023). The Significance of SPP1 in Lung Cancers and Its Impact as a Marker for Protumor Tumor-Associated Macrophages. Cancers *15*. 10.3390/cancers15082250.

61. Myers, J.L. (2012). Hypersensitivity pneumonia: the role of lung biopsy in diagnosis and management. Mod. Pathol. *25 Suppl 1*, S58-67.

62. Kuranishi, L.T., Leslie, K.O., Ferreira, R.G., Coletta, E.A.N., Storrer, K.M., Soares, M.R., and de Castro Pereira, C.A. (2015). Airway-centered interstitial fibrosis: etiology, clinical findings and prognosis. Respir. Res. *16*, 55.

63. Oliver, J.R., Kushwah, R., Wu, J., Cutz, E., Yeger, H., Waddell, T.K., and Hu, J. (2009). Gender differences in pulmonary regenerative response to naphthalene-induced bronchiolar epithelial cell injury. Cell Prolif. *42*, 672–687.

64. Gaunt, J.R., Zainolabidin, N., Yip, A.K.K., Tan, J.M., Low, A.Y.T., Chen, A.I., and Ch'ng, T.H. (2023). Cytokine enrichment in deep cerebellar nuclei is contributed by multiple glial populations and linked to reduced amyloid plaque pathology. J. Neuroinflammation *20*, 269.

65. Liu, Y., Cook, C., Sedgewick, A.J., Zhang, S., Fassett, M.S., Ricardo-Gonzalez, R.R., Harirchian, P., Kashem, S.W., Hanakawa, S., Leistico, J.R., et al. (2020). Single-Cell Profiling Reveals Divergent, Globally Patterned Immune Responses in Murine Skin Inflammation. iScience *23*, 101582.

Fig. 1

A

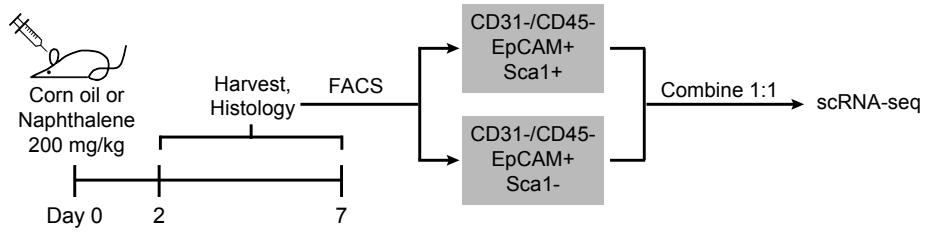

B

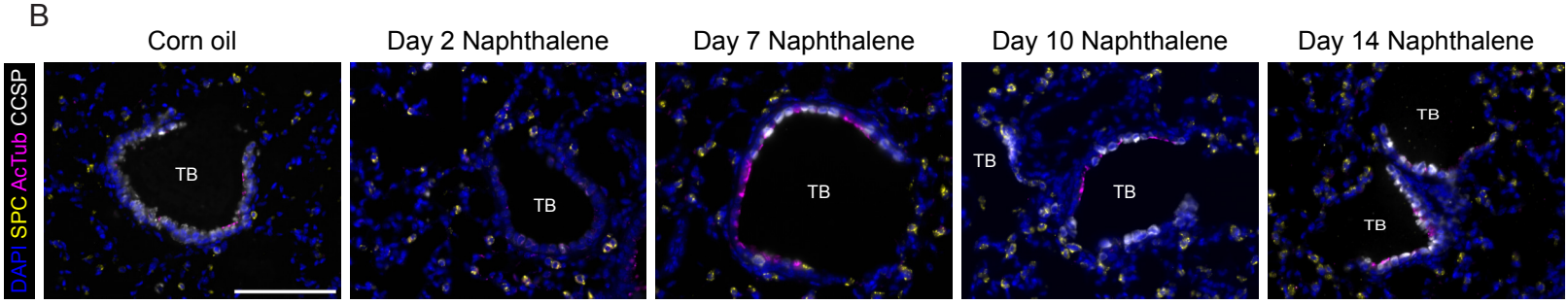

C

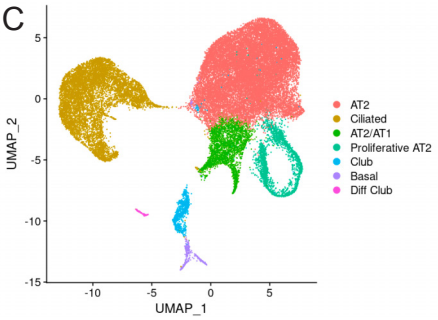

D

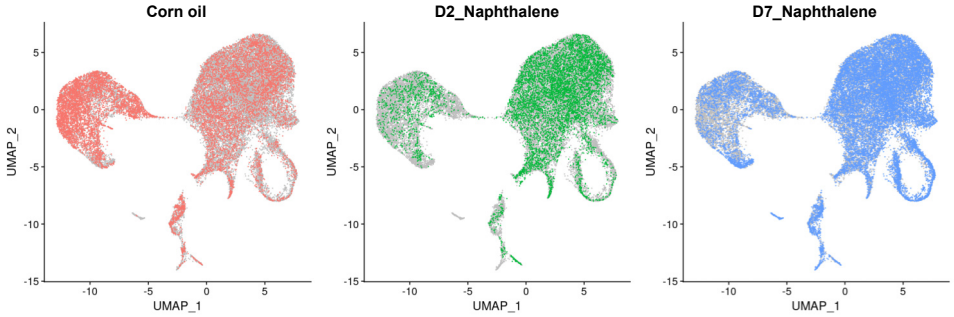

E

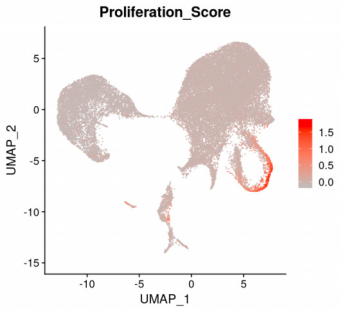

F

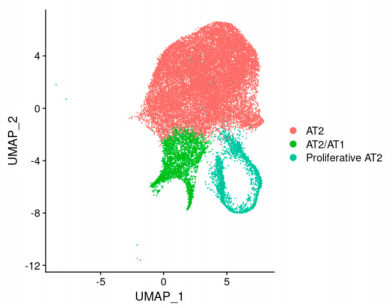

G

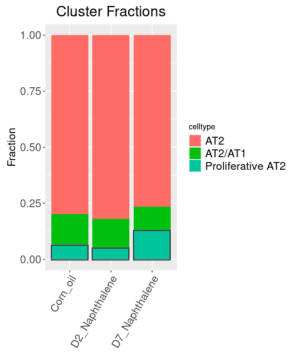

H

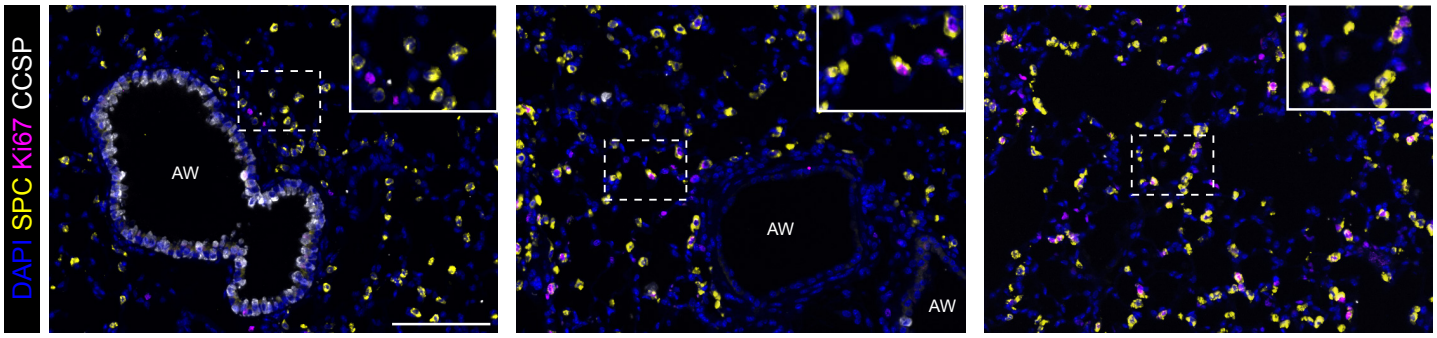

I

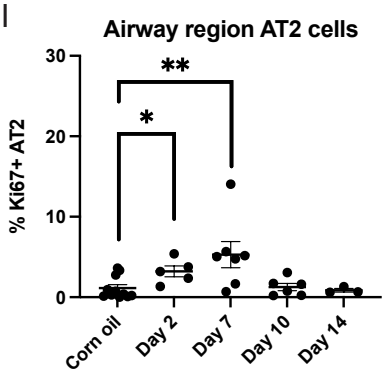

J

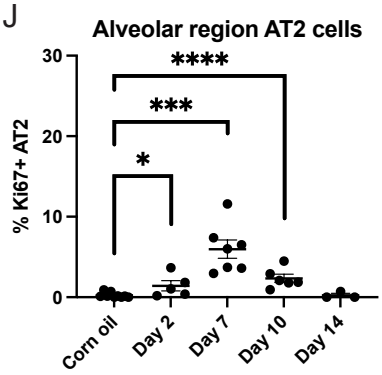

Fig. 2

A

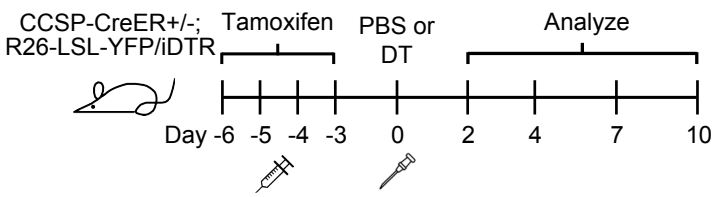

B

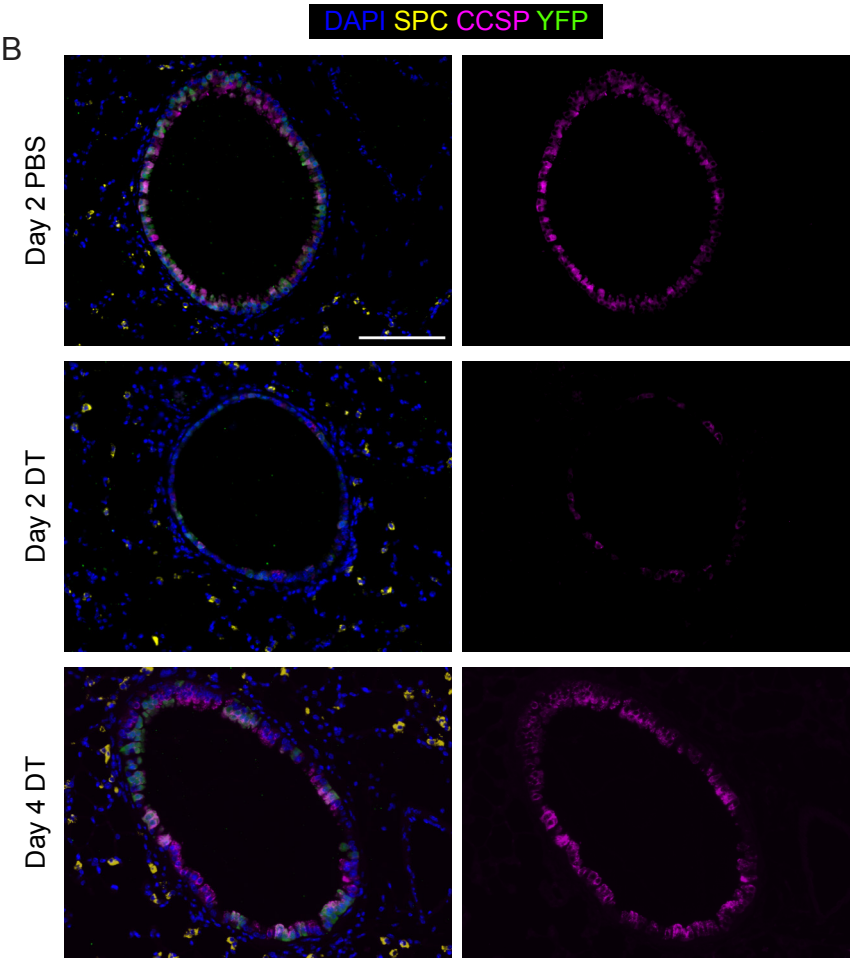

C

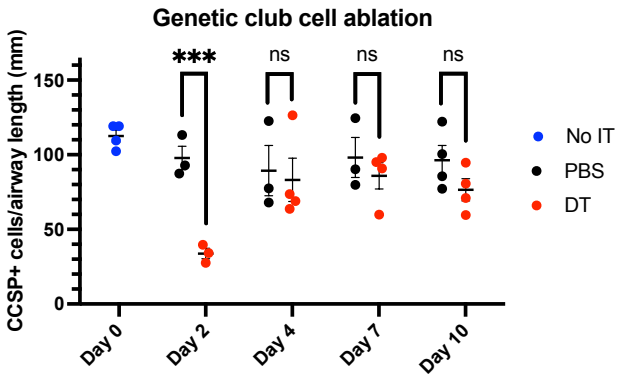

D

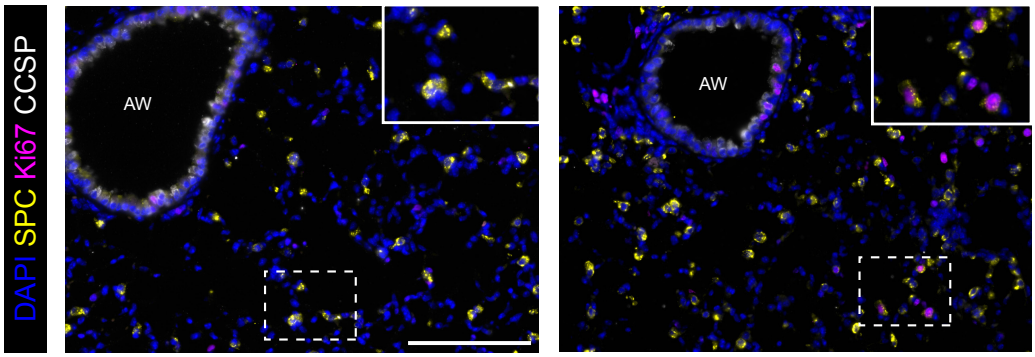

E

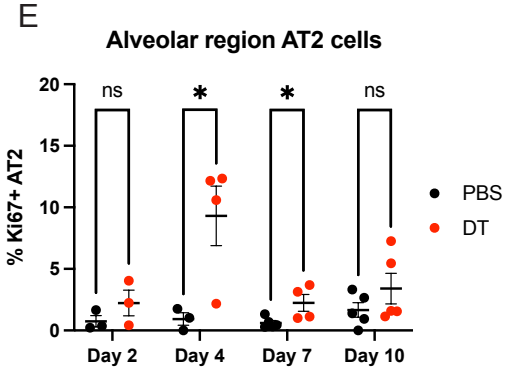

F

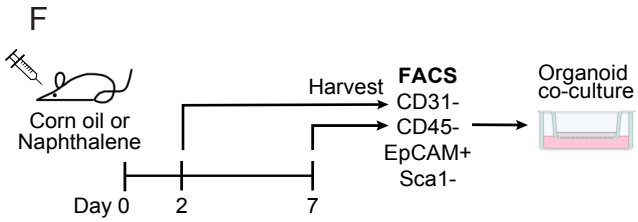

G

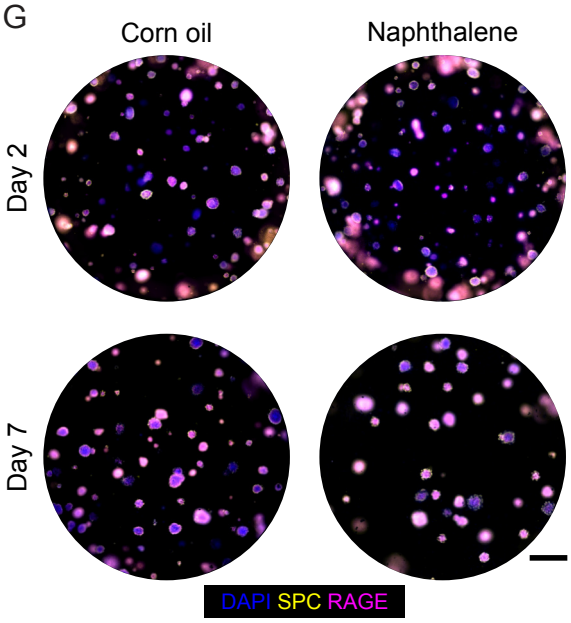

H

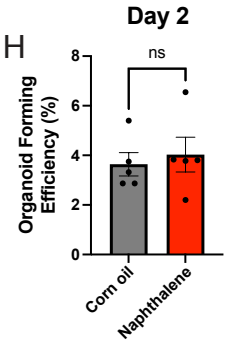

I

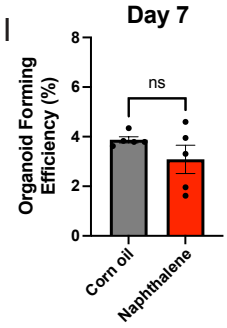

Fig. 3

A

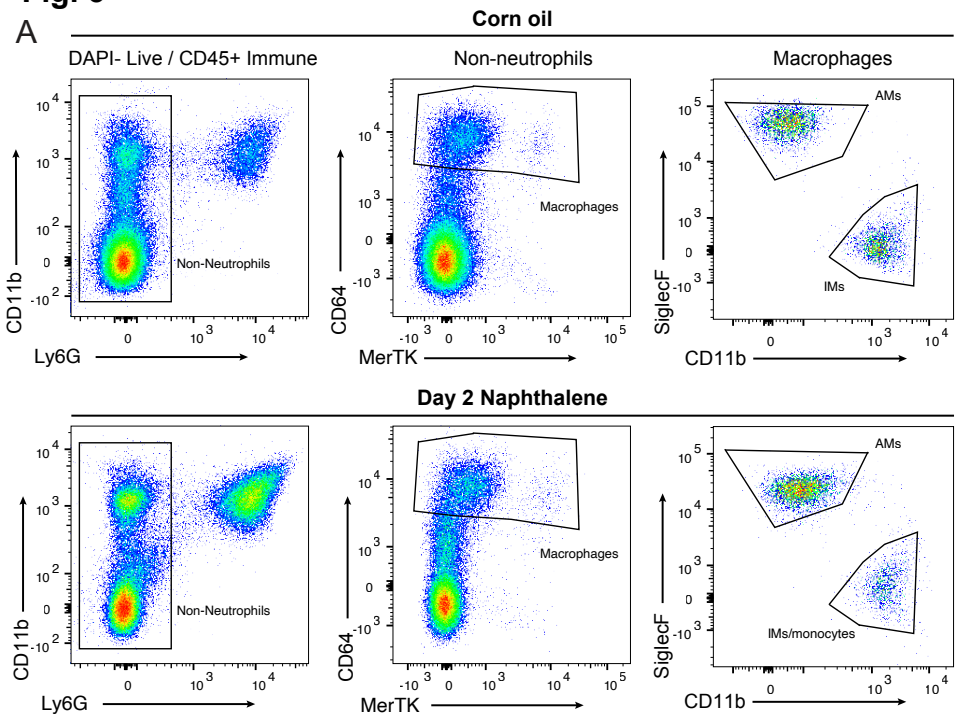

B

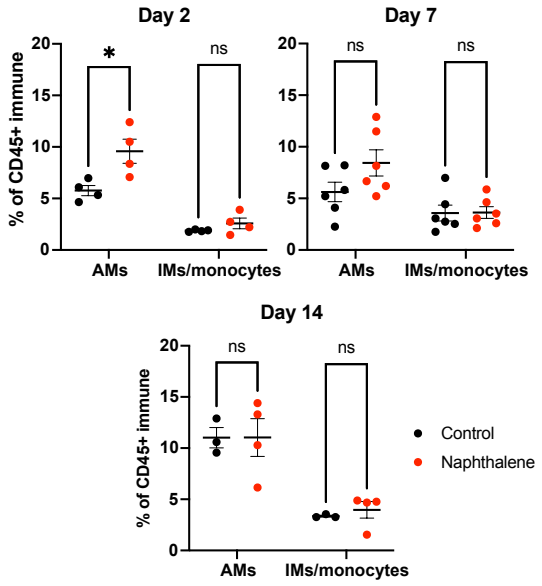

C

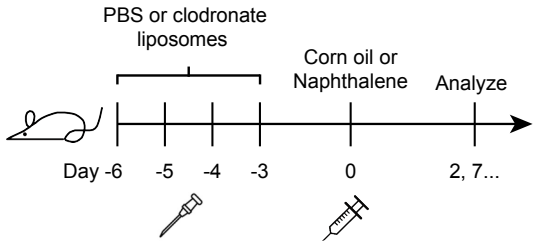

D

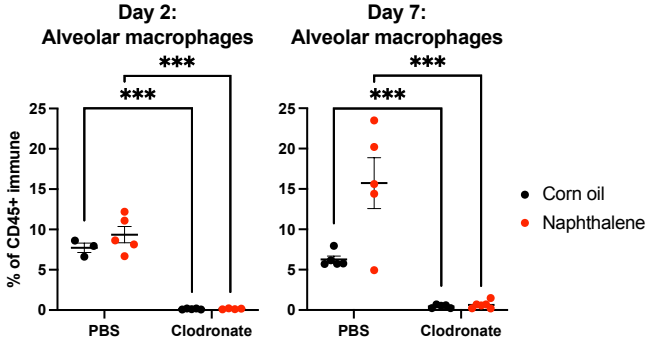

E

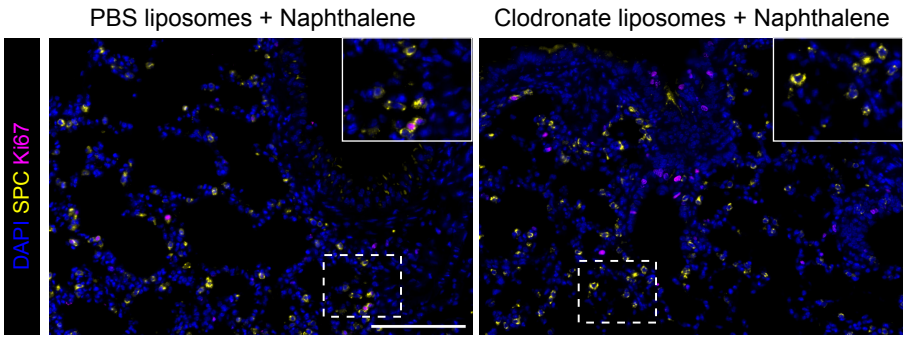

F

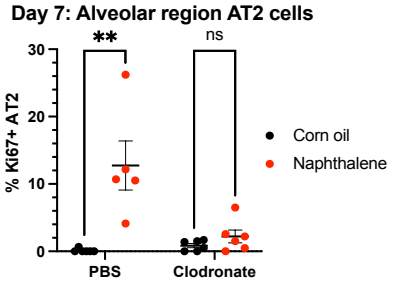

G

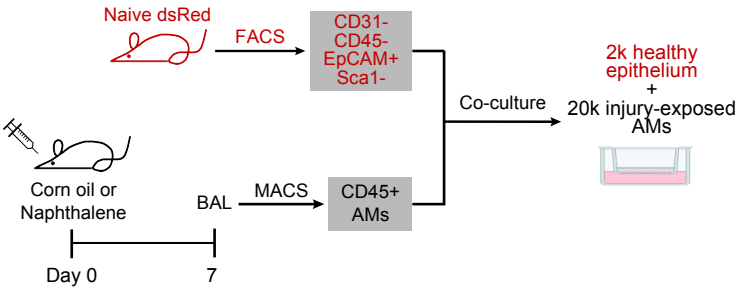

H

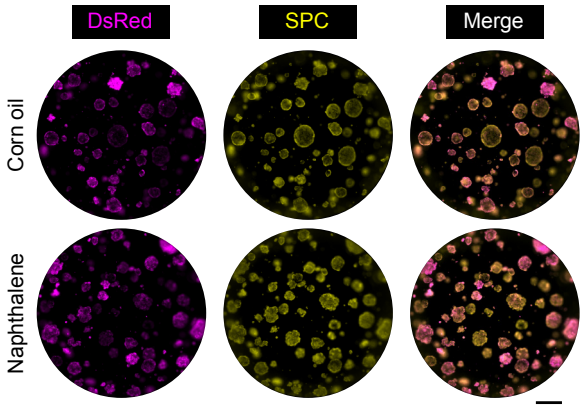

I

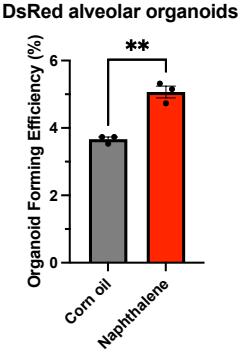

Fig. 4

A

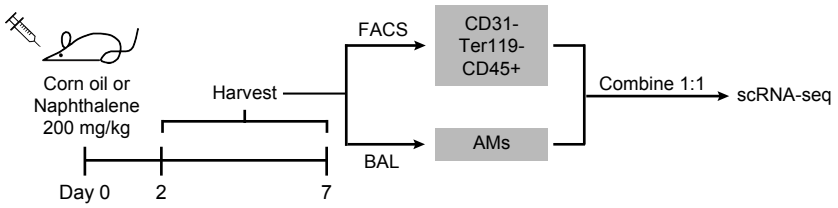

B

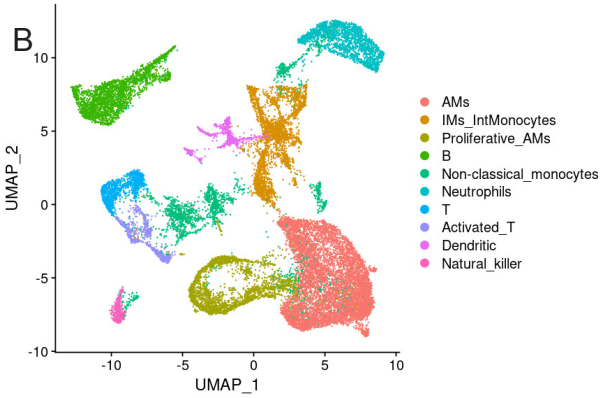

C

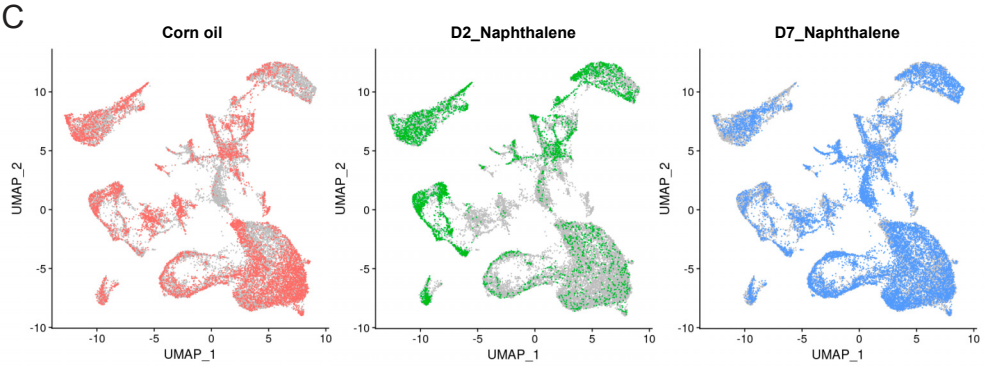

D

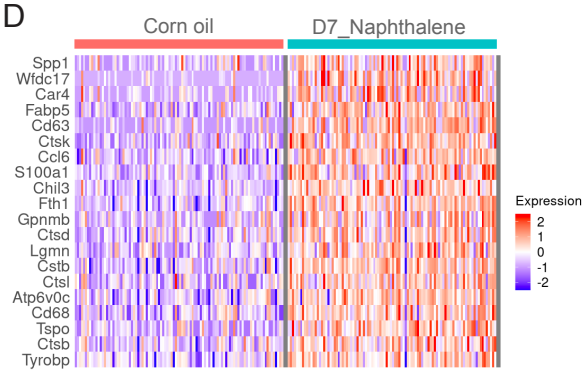

E

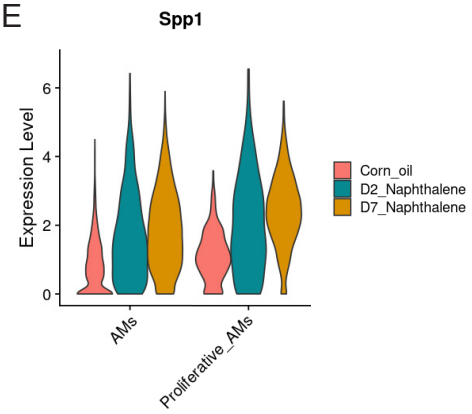

F

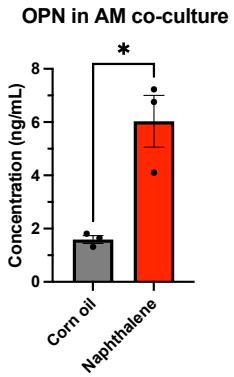

G

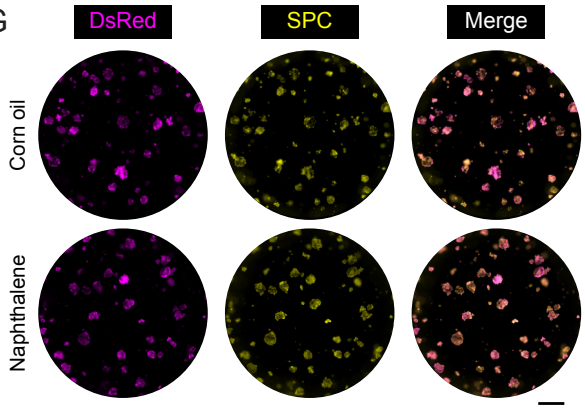

H

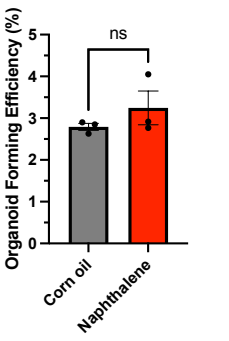

Fig. 5

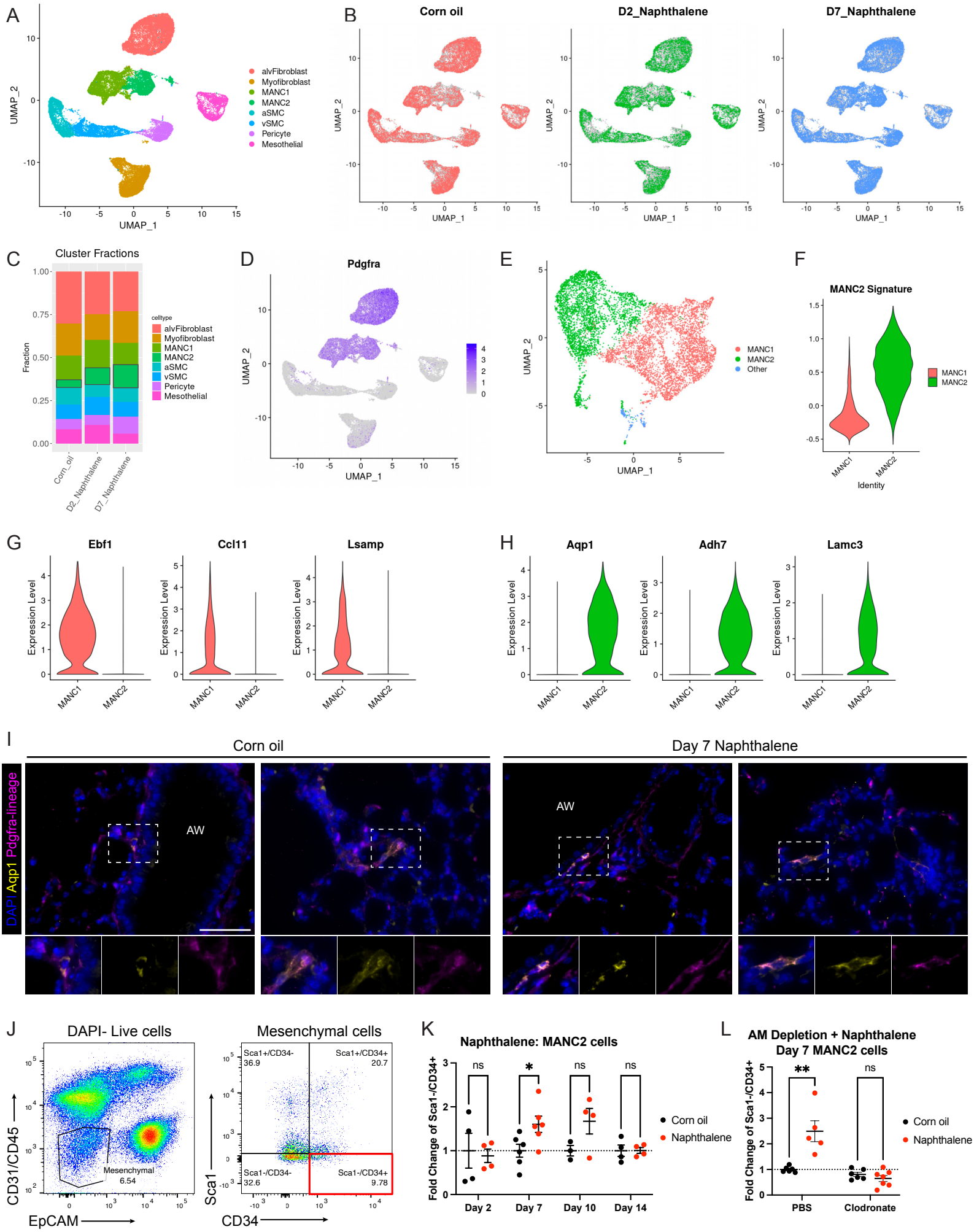
A
UMAP_2
UMAP_1
alvFibroblast
Myofibroblast
MANC1
MANC2
aSMC
vSMC
Pericyte
Mesothelial
B
Corn oil
D2_Naphthalene
D7_Naphthalene
C
Cluster Fractions
Fraction
celltype
Corn_oil
D2_Naphthalene
D7_Naphthalene
D
Pdgfra
E
MANC1
MANC2
Other
F
MANC2 Signature
Identity
G
Ebf1
Ccl11
Lsamp
Expression Level
H
Aqp1
Adh7
Lamc3
I
Corn oil
Day 7 Naphthalene
DAPI Aqp1 Pdgfra-lineage
AW
J
DAPI- Live cells
Mesenchymal cells
CD31/CD45
EpCAM
Mesenchymal
6.54
Sca1+/CD34-
36.9
Sca1+/CD34+
20.7
Sca1-/CD34-
32.6
Sca1-/CD34+
9.78
Sca1
CD34
K
Naphthalene: MANC2 cells
Fold Change of Sca1-/CD34+
ns
*
Day 2
Day 7
Day 10
Day 14
Corn oil
Naphthalene
L
AM Depletion + Naphthalene
Day 7 MANC2 cells
**
PBS
Clodronate